

SUPPORTING INFORMATION

Full-color nanorouter for high-resolution imaging

Mingjie Chen^{1,#}, Long Wen^{1,#}, Dahui Pan¹, David R. S. Cumming², Xianguang Yang^{1,} and Qin Chen^{1,*}*

¹Institute of Nanophotonics, Jinan University, Guangzhou 511443, China

²James Watt School of Engineering, University of Glasgow, Glasgow G12 8QQ, UK

*chenqin2018@jnu.edu.cn, xianguang@jnu.edu.cn

#equal contribution

S1. Nanorouter design with NSGA-II

To optimize the QR-code like distribution of nanoblocks, the genetic algorithm (GA) is applied, which is a global optimization technique inspired by the biological heredity and evolution. GA utilizes a set of binary strings to characterize features of the objectives. During the iteration, the outstanding designs of previous generation are selected based on the fitness and served as parents to generate the next generation. The binary strings of parents would be split and randomly recombined, which is similar to the chromosome division and recombination. Mutation is introduced to increase diversity in order to escape from the local optimal solutions by flipping the value of binary strings. The performance of offspring is evaluated according to the fitness calculated by the defined fitness function. These processes would be repeated until some objectives are met. Following the logic of GA, such a QR-code like distribution of the nanoblocks can be digitalized to a binary $j \times k$ matrix as shown in Figure 1c, where '1' represents the high refractive index nanoblock region and '0' represents the low refractive index environment. Finite-difference time-domain algorithm is applied to solve Maxwell's Equations. Light transmission to silicon diode of each pixel is served as the fitness of the binary structure. To achieve the goal of maximizing transmission for each pixel, NSGA-II as a multi-objective optimized version of GA is applied [1], where a set of non-dominated solutions called Pareto front reach a good trade-off between objectives for each generation. As shown in Figure 2a, each pixel is divided into a 11×11 binary matrix. TiO_2 is chosen as the high refractive index material of nanoblocks. It has been widely used to construct various meta-optics devices in the visible region due to its transparency and relatively high refractive index. The TiO_2 nanoblock layer has a thickness of 600 nm to provide sufficient phase difference for spatial dispersion. Such a high aspect ratio TiO_2 post array has been successively demonstrated in metalens. A SiO_2 spacer is sandwiched between the nanoblocks and the silicon diodes.

S2. Design of nanostructured flat lens

Dielectric planar lens, metalens, plasmonic flat lens are considered for comparison with the proposed QR-code like nanorouter. All these structures have a same aperture size of $3.3 \mu\text{m} \times 1.1 \mu\text{m}$ with a same spacer thickness of 4 μm . The lenses with the propagation phase and the geometric phase have a thickness of 600 nm and a feature size of 100 nm as the nanorouters. The plasmonic lens has a thickness of 50 nm to reduce the transmission loss and a feature size of 50 nm. According to the interference

condition, the local phase at a position r is

$$\varphi(r) = -\frac{2\pi}{\lambda}(\sqrt{r^2 + f^2} - f) \quad (\text{S1})$$

where λ is the wavelength in free space and f is the focal length. The lenses based on the propagation phase and the geometric phase are made of titanium dioxide, while the material of the plasmonic lens based on the resonance phase is aluminum. The structure parameters of all nanoelements in the aperture of all three lenses follows the design in literatures [2-4]. The structure profiles are shown in Figure S1 and the typical structure parameters are given in Table S1.

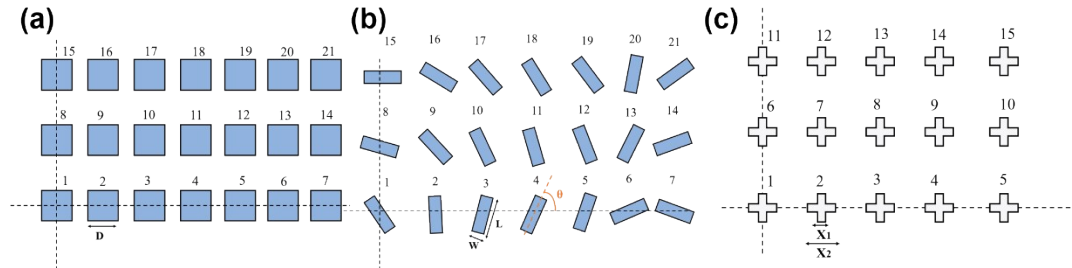


Figure S1. Schematics of (a) dielectric planar lens, (b) metalens ($W = 100$ nm, $L = 250$ nm), (c) plasmonic lens ($X_1 = 50$ nm).

Table S1. Parameters for each nanoblock

Nos.	D (nm)	θ (degree)	X_2 (nm)
1	202	-18.0	192
2	197	-22.5	190
3	190	-35.8	184
4	173	-57.8	177
5	157	-88.3	154
6	139	-126.8	205
7	105	-172.9	198
8	217	-4.5	190
9	212	-9.0	181
10	198	-22.5	171
11	180	-44.7	220
12	162	-75.3	205
13	145	-114.0	192
14	106	-160.4	183
15	220	0.0	172
16	217	-4.5	
17	202	-18.0	
18	182	-40.2	
19	167	-71.0	
20	147	-109.8	
21	110	-156.2	

S3. Polarization dependence of the proposed nanorouter

Apart from the polarization imaging application, the optoelectronic responses of ISs are expected to have no polarization dependence. The dye color filters based on material absorption properties naturally satisfy this requirement. However, the structural schemes including structural color filters and nanorouters may show strong polarization dependence due to the asymmetric design. A *R-G-B* unit cell as shown in Figure 1b is intrinsically asymmetric. To address this issue, each design of the nanorouters is simulated twice under orthogonal polarized incidence respectively. The average transmittance obtained from these two simulations is taken as the fitness in the GA optimization to ensure low polarization sensitivity of the optimal nanorouters. Optical efficiencies of the nanorouter for various polarization angles are shown in Figure S2a-c. It is seen that all the spectra show quite robust profiles for a polarization angle in a range of 0-180°. The spectral correlation coefficients for three color bands shown in Figure S2d keep above 0.9 in all cases indicating the polarization insensitivity of the nanorouter.

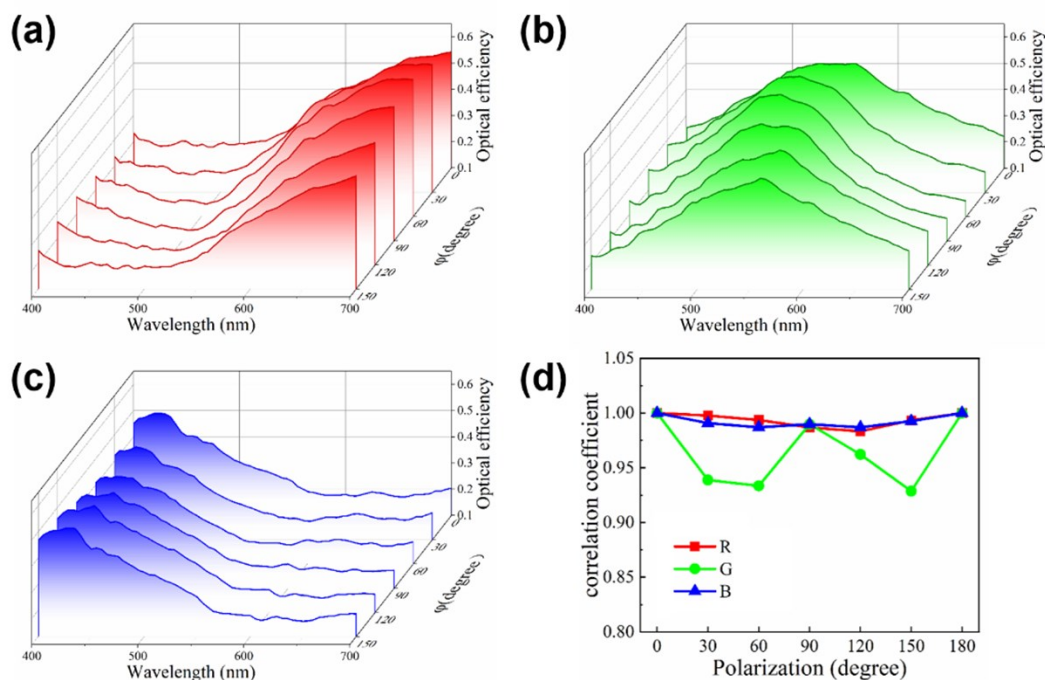


Figure S2. (a)-(c) Optical efficiencies of the nanorouter in *R*, *G* and *B* bands for various polarization angles. (d) Spectral correlation coefficients for various polarization angles. The nanorouter is the same as Figure 3b.

S4. Angular dependence of the color routing performance

All the simulation in the manuscript is at normal incidence. Due to the dispersive property of light scattering, diffraction and interference, the color routing actually presents angular dependence,

which is similar to all color routers and most color filters in literatures [ref. 17, 20, 22-25]. As shown in Figure S3, the spectral correlation coefficients in all color channels (R , G , B) change with the incident angle. Moreover, the angle dependence is more obvious in θ rather than φ . For an incident angle of $\varphi = 5^\circ$, the correlation coefficients in all color channels is close to 1, which means a low angular sensitivity in φ . But for an incident angle of $\theta = 5^\circ$, the correlation coefficient of the spectra of optical efficiency drops to 30%. To reduce the angle dependence, more comprehensive optimization with the consideration of the actual light illumination is required in the future work.

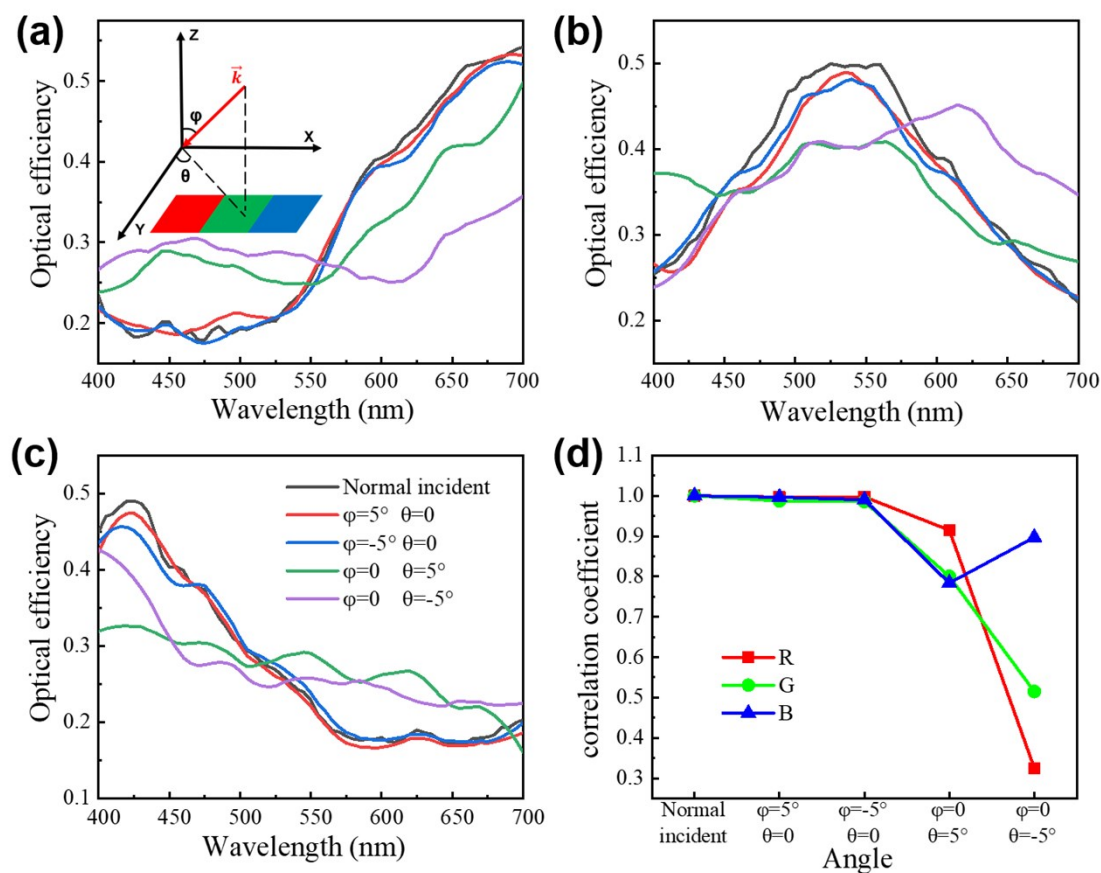


Figure S3. Angle dependence of the color nanorouters in Figure 3. (a)-(c) Spectral responses in R , G and B channels of nanorouters under oblique incidence. (d) Spectral correlation coefficients for various incident angles.

S5. Conversion matrix method for virtual imaging analysis

The actual imaging process can be modeled with a multispectral target image based on a conversion matrix method [5]. First, a multispectral image is selected as shown in Figure 4a and its spatial distribution of the spectral information \mathbf{L} is known. The detected photocurrent vector \mathbf{X} can be calculated by the product of \mathbf{L} and the spectral responses \mathbf{S} of the dye filters or the nanorouters, where \mathbf{S} of the dye

filters is from the commercial product [6] and S of nanorouters is from the FDTD simulation as shown in Figure 3. In digital color imaging, the RGB signal vector Y is converted from the detected photocurrent vector X of R , G and B pixels by a 3×3 conversion matrix A , i.e. $Y = AX$. In principle, the conversion matrix A can be used to convert photocurrent vector X into RGB signal vector Y under any unknown incident illumination. Three rectangular spectra L' in 400nm-500nm, 500nm-600nm and 600nm-700nm are defined to obtain X' , which is applied to solve A with the associated RGB signal vector Y' . The RGB signal vector Y' of three rectangular spectra L' can be obtained base on the CIE Standard Colorimetric System [7]. Thus, the conversion matrix A is solved by numerical algorithms such as the steepest descent method.

To visualize the difference in signal intensities between dye filter and nanorouters, the spectrums of the collected flux in each pixel are integrated. The integral of white light spectrum is supposed to represent the gray value 255. According to this benchmark, the spectral response of each pixel can be linearly converted to gray value in both configurations. The following equations are used to obtain intensities of each pixel for both dye filters and nanorouters.

$$I_{dye} = \frac{\int_{400}^{700} L(\lambda) \mathfrak{S}_{dye}(\lambda) d\lambda}{\int_{400}^{700} d\lambda} \times 255$$

$$I_{router} = \frac{\int_{400}^{700} \frac{L_1(\lambda) + L_2(\lambda) + \dots + L_9(\lambda)}{3} \mathfrak{S}_{router}(\lambda) d\lambda}{\int_{400}^{700} d\lambda} \times 255 \quad (S2)$$

S6. Color nanorouters for sub-micron pixels

The results in Figure 3 and 4 show good performance of the proposed QR-code like color nanorouters for a $1.1 \mu\text{m} \times 1.1 \mu\text{m}$ pixel. As the pixel size of image sensors is scaling down, it is interesting to evaluate the property of such a QR-code like design for a sub-micron pixel. In Figure S4, the calculated optical efficiencies of the nanorouter in R, G and B bands for a pixel of $0.7 \mu\text{m} \times 0.7 \mu\text{m}$ are shown. It is seen that similar color routing performance as Figure 3a is obtained where the optical efficiency is about 50% with a reasonable low cross talk. If the pixel size is further reduced, the nanoblock in a size of $100 \text{ nm} \times 100 \text{ nm}$ may not be feasible any more. Smaller nanoblocks may be required to keep the similar design freedom but the increased aspect ratio of the nanoblocks will be a burden in fabrication. Advanced design or fabrication technique need be developed.

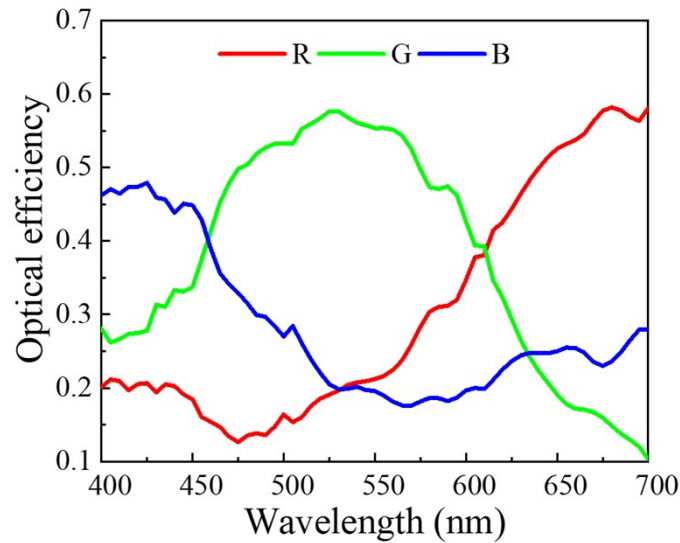


Figure S4. Optical efficiencies of the nanorouter in *R*, *G* and *B* bands for a pixel with a size of $0.7 \times 0.7 \mu\text{m}^2$.

References

1. N. Srinivas and K. Deb, "Multiobjective Optimization Using Nondominated Sorting in Genetic Algorithms," *Evolutionary Computation* **2**(3), 221-248 (1994).
2. M. Khorasaninejad, W. T. Chen, R. C. Devlin, J. Oh, A. Y. Zhu, and F. Capasso, "Metalenses at visible wavelengths: Diffraction-limited focusing and subwavelength resolution imaging," *Science* **352**(6290), 1190-1194(2016).
3. M. Khorasaninejad, A. Y. Zhu, C. R. Cames, W. T. Chen, J. Oh, I. Mishra, R. C. Devlin, and F. Capasso, "Polarization-Insensitive Metalenses at Visible Wavelengths," *Nano Lett.* **16**(11), 7229-7234(2016).
4. L. Lin, X. M. Goh, L. P. McGuinness, and A. Roberts, "Plasmonic Lenses Formed by Two-Dimensional Nanometric Cross-Shaped Aperture Arrays for Fresnel-Region Focusing," *Nano Lett.* **10**(5), 1936-1940(2010).
5. M. Miyata, M. Nakajima, T. Hashimoto, "High-sensitivity color imaging using pixel-scale color splitters based on dielectric metasurfaces," *ACS Photonics* **6**(6), 1442-1450 (2019).
6. H. Taguchi, M. Enokido, "Technology of Color Filter Materials for Image Sensor," in *International Image Sensor Workshop (IISW)* (2011), pp. 34-37.
7. T. Smith, J. Guild, "The CIE colorimetric standards and their use," *Trans. Opt. Soc.* **1931**, 33, 73.